УДК 622.278.66.013; https://doi.org/10.37878/2708-0080/2024-6.12
https://orcid.org/0000-0002-8670-5647
https://orcid.org/0000-0002-1007-1481
https://orcid.org/0000-0001-5960-5678

КОНТРОЛЬ ВЫНОСА ПЕСКА НА КАЗАХСТАНСКИХ НЕФТЯНЫХ МЕСТОРОЖДЕНИЯХ С ИСПОЛЬЗОВАНИЕМ МНОГОФАЗНОЙ CFD-DEM МОДЕЛИ

Ф.А. ХАМИТОВ[1,2],
PhD, постдокторант,
furkhat.khamitov@gmail.com

А.К. КАСЕНОВ[1],
PhD, ассоциированный профессор,
a.kassenov@kbtu.kz

А.А. САРСЕНОВА[1],
магистр, научный сотрудник,
a.sarsenova@kbtu.kz

[1]КАЗАХСТАНСКО-БРИТАНСКИЙ ТЕХНИЧЕСКИЙ УНИВЕРСИТЕТ,
Республика Казахстан, 050000, Алматы, ул. Толе би, 59

[2]УНИВЕРСИТЕТ ААЛТО,
Финляндия, 02150, Эспоо, ул. Кемистинтие 1

Вынос песка является важной проблемой на нефтяных и газовых месторождениях Казахстана со слабосцементированный пластами, в которых присутствует многофазное течение (вода-нефть) пластовых флюидов и твердых частиц. Подход к управлению пескообразованием включает в себя моделирование добычи песка, в частности, многофазный поток жидкости и перемещение частиц в нем. В этом исследовании изучается вынос песка и нефти в многофазном потоке с использованием сопряженного моделирования вычислительной гидродинамики и метода дискретных элементов (CFD-DEM) на образце кубического песчаника с акцентом на традиционную вертикальную добывающую скважину. Модель слабосцементированного песчаника использовалась для моделирования выноса частиц песка из Объекта 2 нефтяного месторождения Каражанбас. Были смоделированы четыре случая с разными размерами фильтра и один вариант без фильтра. Размеры сеток фильтра были выбраны на основе распределения размеров частиц образца. Наблюдалось переходное поведение выноса песка при моделировании без фильтра, которое показало качественное соответствие литературным данным. Размер отверстия фильтра существенно влияет на вынос песка, при этом фильтры с малым отверстием способствуют

большему снижению выноса песка. Эффективный контроль песка был достигнут при диаметрах сита до 3d50 (средний диаметр частиц), при дальнейшем увеличении наблюдался значительный вынос песка. Внедрение фильтра имело мультипликативный эффект: контроль выноса песка и повышение коэффициента извлечения нефти до 21%.

КЛЮЧЕВЫЕ СЛОВА: *вынос песка, CFD-DEM, слабосцементированный песчаник, многофазная жидкость, вторичный метод повышения нефтеотдачи, взаимодействие жидкости и твердого тела.*

КӨПФАЗАЛЫ CFD-DEM МОДЕЛІН ҚОЛДАНУ АРҚЫЛЫ ҚАЗАҚСТАННЫҢ МҰНАЙ КЕН ОРЫНДАРЫНДА ҚҰМ ӨНДІРУ ПРОЦЕСІН БАҚЫЛАУ

Ф.А. ХАМИТОВ[1,2], PhD, постдокторлық зерттеуші, *furkhat.khamitov@gmail.com*
А.К. КАСЕНОВ[1], PhD, қауымдастырылған профессор, *a.kassenov@kbtu.kz*
А.А. САРСЕНОВА[1], магистр, ғылыми көмекші, *a.sarsenova@kbtu.kz*

[1]ҚАЗАҚ-БРИТАН ТЕХНИКАЛЫҚ УНИВЕРСИТЕТІ,
Қазақстан Республикасы, 050000, Алматы, Төле би, 59

[2]ААЛТО УНИВЕРСИТЕТІ,
Финляндия, 02150, Эспоо, Кемистит 1

Құм шығару Қазақстанның әлсіз шоғырландырылған түзілімдерінде көп фазалы (сұмұнай) қабат сұйықтықтары мен қатты бөлшектердің ағыны бар мұнай-газ кен орындарында маңызды мәселе болып табылады. Құмды бақылау тәсілі құм өндірудің көп масштабты механизмдерін, әсіресе сұйықтық ағыны мен бөлшектердің қозғалысын қамтиды. Бұл зерттеуде тік ұңғымасына назар аудара отырып, көп фазалы ағындағы құм өндірісі және мұнай өндіру текше құмтас үлгісінде Сұйықтықтын Есептеу Динамикасы және Дискретті Элементтер Әдісін (CFD-DEM) біріктіріп модельдеу арқылы талдайды. Әлсіз құмтас түзілімдерінің моделі Қаражанбас кен орнының 2 нысанынан құм бөлшектерін шығару процесін модельдеу үшін қолданылды. Әртүрлі електермен және електерсіз төрт жағдай модельденді. Електердің өлшемдері үлгі бөлшектерінің таралуы (PSD) негізінде таңдалды. Елексіз модельдеу кезінде құм өндірудің өтпелі әрекеті байқалды және әдебиеттермен сапалы келісімді көрсетті. Електің мөлшері құмның шығарылуына айтарлықтай әсер етеді, ал кішігірім електер экстракция жылдамдығын төмендетеді. Құмды тиімді бақылау диаметрлері 3d50 (бөлшектердің орташа диаметрі) өлшемдегі електермен қол жеткізілді, олардың одан әрі ұлғайтуы құм кетуіне жол бермеді. Електерді қолдануы құм өндірісін тиімді бақылауға және мұнай алу коэффициентін 21% - ға дейін арттыруға мүмкіндік берді

ТҮЙІН СӨЗДЕР: *Құм өндіру, CFD-DEM, әлсіз цементтелген құмтас, көпфазалы сұйықтық, мұнайды алудың қайталама күшейтілген әдістері, сұйықтық пен қатты заттың әрекеттесуі.*

SAND PRODUCTION CONTROL IN KAZAKHSTAN OILFIELDS USING A MULTIPHASE CFD-DEM MODEL

F. KHAMITOV[1,2], PhD, Postdoctoral researcher, *furkhat.khamitov@gmail.com*
A. KASSENOV[1], PhD, Associate Professor, *a.kassenov@kbtu.kz*
A. SARSENOVA[1], MS, Research assistant, *a.sarsenova@kbtu.kz*

[1]KAZAKH-BRITISH TECHNICAL UNIVERSITY,
Tole Bi Street 59, Almaty, 050000, Kazakhstan

[2]AALTO UNIVERSITY,
02150 Espoo, Kemistintie 1, Finland

Sand production is a significant issue in Kazakhstan's oil and gas fields with unconsolidated formations involving the multiphase flow (water-oil) of reservoir fluids and solid particles. The sand control approach includes the multiscale mechanisms of sand production, particularly fluid flow and particle movement. This study investigates sand production and oil recovery in multiphase flow using coupled Computational Fluid Dynamics and Discrete Element Method (CFD-DEM) modeling on a cubic sandstone sample, focusing on a traditional vertical producing well. The weak sandstone formations model was used to simulate sand particle extraction from Object 2 of the Karazhanbas oilfield. The four cases with different sieve sizes and one without sieve were simulated. The sieve sizes were chosen based on sample particle size distribution (PSD). The transient sand production behavior in simulations without a sieve was observed and showed qualitative agreement with the literature data. Sieve size significantly impact sand production, with smaller sieves reducing extraction rates. Effective sand control was achieved with sieve diameters up to 3d50 (average particle diameter), beyond which further increases did not prevent sand production. The sieve implementation had a multiplicative effect: controlling sand production and improving the oil recovery factor by up to 21%.

KEY WORDS: *Sand production, CFD-DEM, weak formation, multiphase fluid, secondary EOR, fluid-solid interaction.*

Introduction. Oil and associated gas production from reservoirs with weakly consolidated or unconsolidated formations is frequently associated with sand production. This issue is common in many oil fields in Kazakhstan, including Karazhanbas, North Buzachi, Kalamkas, Zhalgiztobe, Kenkiyak and Uytas. Understanding and predicting the sand production process is one of the primary challenges to ensuring safe and profitable hydrocarbon production in Kazakhstan and globally. Sand production can significantly reduce production flow rates, cause damage to both downhole and surface equipment, and increase the likelihood of critical failures. However, extracted sand material from the reservoir can increase the porosity close to the wellbore. Thus, a zone of increased permeability can be formed, which positively increases the liquid production flowrate [1-2].

Veeken et al. (1991) grouped the parameters influencing sand production into three categories (*see Tab.1*): the physical properties of the reservoir formation and the fluid, the well installation and completion, and the type of oil and gas field development [3].

In the long-term well exploitation, the amount of produced sand will depend on the reservoir management. Still, local sand production can be prevented only by installing of downhole sand control systems such as gravel packs, sand screens and chemical consolidations, which could inhibit the movement of sand into the underground and surface facilities [4]. However, each method comes with its risks, so selecting the appropriate sand control solution for a specific formation is crucial. The sand control strategies depending on porosity values were discussed by Ben Mahmud et al. (2020). Choosing optimal screen size is still challenging and requires information about sand size distributions, rock strength, type of fluids and so on [5-6].

Table 1 – **Parameters influencing sand production [3]**

FORMATION	
Rock	· Strength
	· Vertical and horizontal in-situ stresses (change during depletion)
	· Depth (influences strength, stresses and pressures)
Reservoir	· Far field pore pressure (changes during depletion)
	· Permeability
	· Fluid composition (gas, oil, water)
	· Drainage radius
	· Reservoir thickness
	· Heterogeneity
COMPLETION	
· Wellbore orientation, wellbore diameter	
· Completion type (open hole/perforated)	
· Perforation methods (height, size, density, phasing, under/overbalance)	
· Sand control (screen, gravel pack, chemical consolidation)	
· Completion fluids, stimulation (acid volume, acid type)	
· Size of tubulars	
PRODUCTION	
· Flow rate	
· Drawdown pressure	
· Flow velocity	
· Damage (skin)	
· Bean-up/shut-in policy	
· Artificial lift technique	
· Depletion	
· Water/gas coning	
· Cumulative sand volume	

Kazakhstan oil fields with weak sandstone reservoirs are characterized as highly permeable and porous with initial water content above 20%, low depth of occurrence, and high oil viscosity. The watercut in producing wells increases during the well life [7-9]. A typical producing well history with sand production in the Ustyurt-Buzachi sedimentary basin is illustrated in *Figure 1* [10]. The sandrate or sandcut is reducing from the initial high to the small constant values, while the watercut is only increased.

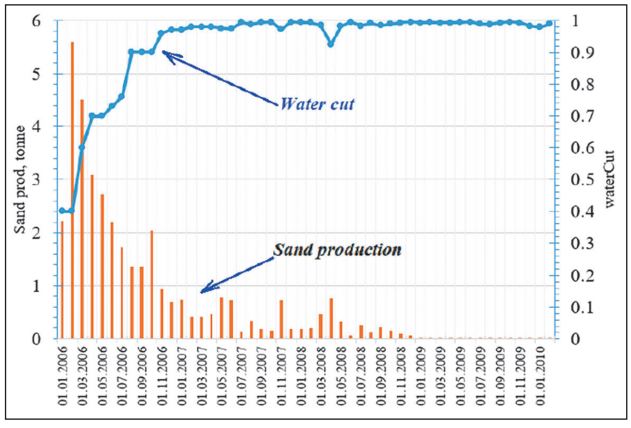

Figure 1 – **Sand production pattern in Ustyurt-Buzachi basin [10]**

The CFD-DEM approach for sand production was introduced by Tsuji et al. (1993) to investigate the particle motions in a 2D gas-fluidized bed system [11]. Zhou et al. (2011) developed a combined 3D CFD-DEM model, demonstrating that this approach can effectively simulate sand erosion in weak formations. They emphasized that the fluid-particle interaction force plays a crucial role in driving sand production [12]. One of the critical parts of CFD-DEM modelling of weak reservoir formation is correctly calibrating digital DEM rock by real reservoir sand properties from Kazakhstan oilfields. This investigation can be found in the literature [13]. The mechanisms of underpinning sand production under different flow conditions of a single fluid for the cylindrical sample have been investigated by Khamitov et al. (2021, 2022) in micro-scale [10, 14-15] and for cubic spacemen in meso-scale by Kazidenov et al. (2022) [16].

This study conducted the multiphase CFD-DEM modelling on a micro-scale for Object 2 of the Karazhanbas oil field's reservoir condition in different sizes. The effect of sieve size on sand production and oil recovery was investigated.

Numerical Formulation. The CFD-DEM model based on the Euler-Lagrange scheme, where a continuous fluid flow is coupled with discrete particles by exchanging momentum, energy, and mass terms. The model considers particle modeling particles at the micro-scale and fluid at the meso-scale [11-12, 17].

Governing equations for DEM particles. DEM has been extensively used to investigate the mechanics of granular flow, as pioneered by Cundall et al. [18]. Particles within a computational domain are explicitly tracked by solving governing particle motion equations. This provides detailed information on the interparticle contact forces and particle trajectories. Different materials can be simulated using DEM by specifying the physical properties of particles and contact model parameters, which allows for various configurations of linear and nonlinear elastoplastic behavior [19]. Cemented rock material can also be modeled as an assembly of fully or partially bonded particles. The bonding force was included in calculating contact forces and the particles' translational and angular accelerations. In this study, the cemented contacts were modeled using the modified JKR contact model [14-15].

In CFD-DEM simulation, the particle phase is coupled with a fluid phase. The numerical model takes into account particle-particle and fluid-particle interaction forces in Newton's second law that governs particle motion. For any particle p [20]:

$$m_p \frac{d\vec{u}_p}{dt} = \vec{f}_{p,n} + \vec{f}_{p,t} + \vec{f}_{p,f} + \vec{f}_{p,Pres} + \vec{f}_{p,vis}, \quad (1)$$

$$I_p \frac{d\vec{\omega}_p}{dt} = r_{p,c} \times \vec{f}_{p,t}, \quad (2)$$

Here, m_p denotes the particle mass, the linear velocity is $\bar{u}_p$, and $r_{p,c}$ refers to the radius of the particle. The normal and tangential contact forces between particles are $\bar{f}_{p,n}$ and $\bar{f}_{p,t}$, respectively, $\bar{f}_{p,f}$ represents the drag force exerted on the particle from the fluid phase, Additionally, $\bar{f}_{p,Pres}$ denotes the pressure force, $\bar{f}_{p,vis}$ represents the viscous force. The $\bar{\omega}_p$ is angular velocities and I_p represents the moment of inertia.

The pressure force $\vec{f}_{p,Pres}$ can be define as:

$$\vec{f}_{p,Pres} = -\nabla P \cdot V_p \tag{3}$$

where ∇P is the fluid pressure gradient and V_p is volume of particles.

The viscous force $\vec{f}_{p,,vis}$ can be calculated as:

$$\vec{f}_{p,vis} = -(\nabla \cdot \bar{\bar{\tau}})V_p \tag{4}$$

where $\bar{\bar{\tau}}$ is the fluid stress tensor (see Eq. 6).

Eq. 1 describes the translational motion, while Eq. 2 is used to describe the rotational motion of particle p. In the absence of the liquid phase, the fluid-related force terms ($\vec{f}_{p,f}$, $\vec{f}_{p,Pres}$, $\vec{f}_{p,vis}$) are equal to zero. The contact forces between particles, $\vec{f}_{p,n}$ and $\vec{f}_{p,t}$, were calculated using the modified JKR contact model [14-15].

Governing equations for CFD-DEM interaction. The CFD-DEM coupling in this study was based on model A, as described in literature [17,20]. The modified Navier-Stokes equations and the interface tracking Volume of Fluid (VOF) method [21] were employed to describe the governing equations of two-phase fluid flow (water and oil) in the presence of a third particulate phase (sand particles). The CFD-DEM-VOF method has already successfully implemented in multiphase studies and validated by well-known benchmark tests [22]. The unresolved CFD-DEM model (fluid phase is not resolved at the particle scale), with VOF can be formulated as follows:

$$\begin{cases} \dfrac{\partial(\varepsilon_f \alpha_w)}{\partial t} + \nabla \cdot (\varepsilon_f\, \alpha_w \vec{u}_f) - \nabla \cdot (\vec{u}_c\, \alpha_w \alpha_o) = 0 \\ \dfrac{\partial(\varepsilon_f)}{\partial t} + \nabla \cdot (\varepsilon_f \vec{u}_f) = 0 \\ \alpha_w + \alpha_o = 1 \\ \dfrac{\partial(\varepsilon_f \rho_f \vec{u}_f)}{\partial t} + \nabla \cdot (\varepsilon_f \rho_f \vec{u}_f \vec{u}_f) = -\varepsilon_f \nabla P - \vec{F}^A_{pf} + \varepsilon_f \nabla \cdot \bar{\bar{\tau}} + \varepsilon_f \rho_f \vec{g} \end{cases} \tag{5}$$

Here, the volume fraction occupied by the fluid is represented by ε_f, while α_w and α_o refer to the volume fraction of water and oil, respectively. The compression velocity at the interface between the phases is denoted as $\bar{u}_c$, where $\bar{u}_c = \bar{u}_{f,w} - \bar{u}_{f,o}$. Additionally, other variables include $\bar{u}_f$, which represents fluid velocity, ρ_f for fluid density, P for pressure, $\bar{F}^A_{pf}$ for volumetric particle-fluid interaction force, $\bar{g}$ for gravity vector, and t for time. The stress tensor $\bar{\bar{\tau}}$ is obtained for fluid with viscosity μ_f as:

$$\bar{\bar{\tau}} = \mu_f(\nabla \vec{u}_f + \nabla \vec{u}_f^T) - \frac{2}{3}\mu_f I \nabla \cdot \vec{u}_f \tag{6}$$

In contrast to the Euler-Euler two-fluid approach, the Volume of Fluid (VOF) method assumes the absence of interaction forces between fluid phases and solves only a single momentum and continuity equation through employing the fluid-mixture properties that are weighted by volume:

$$\rho_f = \alpha_w \rho_w + \alpha_o \rho_o \tag{7}$$

$$\mu_f = \alpha_w \mu_w + \alpha_o \mu_o \tag{8}$$

The volumetric particle–fluid interaction force $\bar{F}_{pf}^{A}$ is determined as:

$$\vec{F}_{pf}^{A} = \frac{1}{\Delta V}\sum_{p=1}^{n}(\vec{f}_{p,f}) \quad (9)$$

$$\vec{f}_{p,f} = \vec{f}_{p,d} + \vec{f}_{p}'' \quad (10)$$

Here, the term ΔV represents the volume of the fluid cell, while n denotes the number of particles in the computational cell. $\bar{f}_{p,d}$ represents the drag force. Additionally, $\bar{f}_{p}''$ refers to the sum of particle-fluid interaction forces acting on particles other than the drag force. These forces are related to pressure gradient and viscous stress and are commonly regarded as the dominant forces in particle-fluid flow.

The interactions between the fluid and the particle phases were simulated by a four-way coupling method. Four-way coupling in the CFD-DEM simulations aims to capture the intricate interplay between fluid and particle phases in a system, considering both direct and indirect interactions among particles and between particles and the surrounding fluid. The motion of particles affects the motion of fluid and vice versa. Three forces were considered in the coupling information: pressure force, viscous force and the Di Felice drag force [23]. The Di Felice drag formulation assumes spherical particles, which do not interact with each other and neglects the effects of particle shape and size variation on drag force. Taking into account the continuity and precision of the different drag force calculation models, the Di Felice model provided more accurate calculations for dense particle systems. Therefore, this drag model has been chosen for the current study. Further information can be found in previous papers [14-15].

Sand production simulation procedure. The coupled simulation was carried out in several stages. Initially, a sandstone sample was created through particle pluviation, compressional diagenesis, and cementation in cubic spacemen. A perforation was made in the sample to form a horizontal channel running through its full width, connecting to an outlet at the center of the right surface. The oil phase was introduced into the solid phase after forming the CFD mesh, which matched the dimensions of the perforated sandstone sample. The injected water from the left side flowed through the granular sample towards the right outlet, with the perforation channel accelerating the flow.

DEM sample preparation and perforation. The DEM model used for the dry sample (no liquid phase) was similar to previous works [14-15]. Eight different size particles were randomly generated and allowed to fall under gravity (pluviation) inside a cubic container. The Particle Size Distribution (PSD) of the numerical sample was selected to match that of a real sandstone from the Ustuyrt-Buzachi sedimentary basin, as reported by Shabdirova et al. (2016) [24]. The total number of particles was 434822, which corresponded to a sample mass of 6.87 g with size d50 (mean particle size of the sample) about 0.2294 mm (*Tab. 2*).

The micromechanical properties of sand material for DEM were used similar to previous studies [13, 15-16]. The top wall was moved downwards to compress the particles until a vertical stress of 5.9 *MPa* was attained, resulting into an intact sample with a width (*a*) of 16.8 *mm* and a height (*h*) of 15.15 *mm*. The axial cross section of compressed sample is shown in *Figure. 2*.

Table 2 – **Particles groups in the cubic sample**

Diameter of particle *(mm)*	0,15	0,18	0,2	0,22	0,25	0,275	0,3	0,355 *(dmax)*
Particle number in group	90243	67505	58031	60098	76137	43143	23559	16106
Mass ratio *(%)*	5.81	7.5	8.85	12.2	22.68	17.1	12.13	13.74
Particle mass *(g)*	0.399	0.515	0.608	0.838	1.557	1.174	0.833	0.943

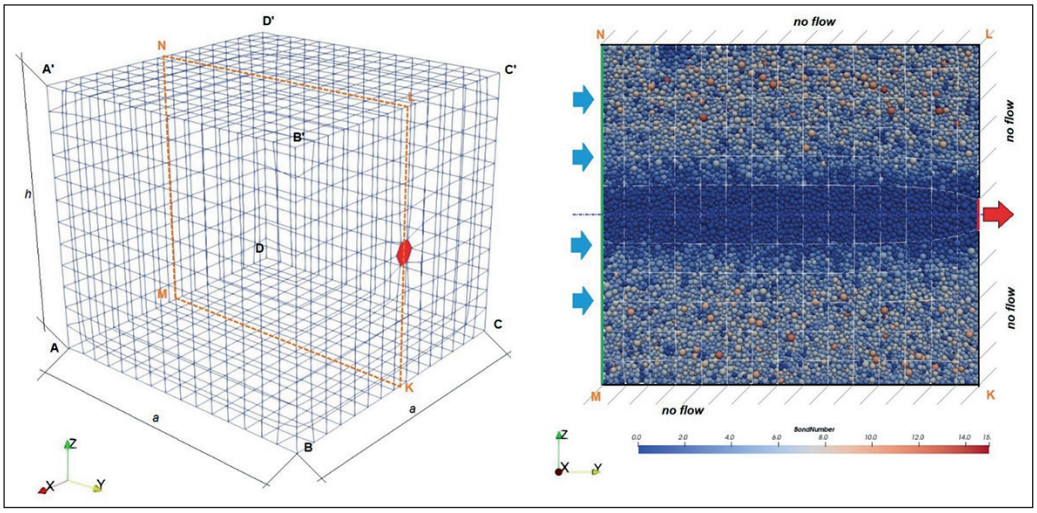

Figure 2 – **CFD mesh (left) and DEM sample (right)**

Particles in the sandstone sample could develop multiple contacts with their surrounding neighbors. In its intact state, all bonded contacts were formed at once using the modified JKR model [14-15]. This model agrees well with the experimental study with unconsolidated sandstone from the Ustyurt-Buzachi sedimentary basin [10, 24]. Perforation was simulated by driving a penetrometer with diameter of 1.4 *mm* horizontally into the sample and then withdrawn. Particle bonds were destroyed in this process, and this resulted in a damage region of unbonded particles in the middle of the sample as shown in *Figure 2*. Further information can be found in similar simulations [14-15].

CFD-DEM simulation. Sand production simulation was conducted by water injection and producing sand particles at outlet, the particles moved toward outlet under the influence of the injecting water and were deleted once they exited the outlet. Numerical simulations of multiphase fluids were conducted to examine the different DEM outlet (sieve sizes). Water flow was injected on the left inlet surface (*AA'D'D*) with constant velocity about $2.83 \cdot 10^{-2}$ *m/s* (*Figure 2*).

The coupled CFD–DEM formulation in Eq.5 was implemented as model A in the commercial CFDEM®coupling program. The CFDEM program is a highly parallelized computational platform that combines the Aspherix® program for the DEM modeling and the open-source OpenFOAM-8 program for the CFD modeling. The numerical simulations in this study were executed on a High-Performance Computer System, which was equipped with 52 multi-threading processors Intel Xeon® Gold 6230R with a clock speed of 2.1

GHz and 503 GB of memory. A typical simulation of 0.3 s of physical time could take about 24 days to complete even with the parallel computation that utilized as many as 12 threads using the Message Passing Interface (MPI) protocol.

The CFD mesh grid was developed using the HELYX-OS graphical user interface. The computational fluid domain in *Figure 2* (left) has 2700 cells that formed the same dimensions of the DEM sample. The CFD mesh cell Δx_{cfd} equal to $11.2 \cdot 10^{-4}$ *m* was chosen similarly to Khamitov et al. (2022) to achieve the mesh-independent solution, where the accuracy of the simulation is still acceptable, and computation speed is maximized. The ratio between the size of CFD mesh and the maximum particle diameter is equal to 3.15. The divided void fraction model was used for fluid fraction calculation in CFD cell.

The Object 2 of the Karazhanbas oil field's reservoir properties was chosen for initial and boundary conditions of the CFD-DEM simulations. The Object 2 is at a depth 290 *m* with initial reservoir pressure 4.5 MPa. The average calculated overburden stress for this Horizon G is found as 5.9 MPa [8]. The all CFD walls in *Figure 2* (left) were impermeable with a no-slip condition. A central "red" zone on the center of surface (BB'C'C) served as the fluid outlet. The injecting water and saturating oil were assumed as incompressible. The fluid properties are tabulated in *Table 3*. The different DEM holes are implemented at outlet to simulate sieve affect.

Table 3 – **Typical reservoir fluid properties for heavy oil and unconsolidated sandstone**

Reservoir fluid	Kinematic viscosity, m^2/s	Density, kg/m^3
Heavy Oil	$387{,}2 \cdot 10^{-6}$	940
Water	$1 \cdot 10^{-6}$	1000

The DEM and CFD simulations used discretization time steps of $2 \cdot 10^{-8}$ s and $2 \cdot 10^{-7}$ s, respectively. To synchronize the two simulations, the CFD simulation was run every 10-time steps of the DEM simulation, which allowed for accurate and efficient two-way coupling data exchange. The DEM simulation provides the locations of each particle for the calculating of the fluid volume fraction ε_f and the particle–fluid interaction force $\bar{F}^A_{pf}$ in each CFD cell (Eq. 5). The updated fluid pressure and velocity affect particle gradient pressure, viscous, and drag forces.

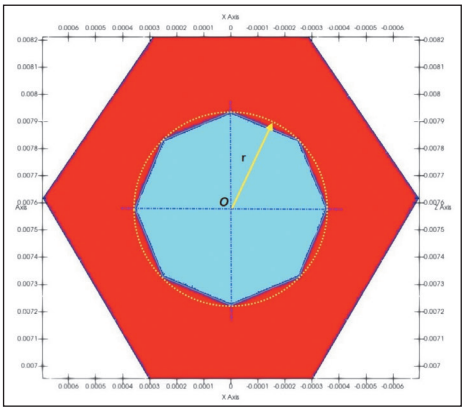

Figure 3 – **Impermeable perforated DEM wall (red) with hole for particle extraction (sky blue)**

The different sieve sizes were implemented by introducing perforated DEM walls at the outlet (*Figure 3*). Fluid boundary conditions didn't change, but the DEM simulation conditions varied. The perforated hole radius is r = 1.5; 2;2.5;3 * *dmax/2*, where *dmax* is maximum particle diameter in the sample (*Tab. 2*).

Results and Discussion. Five numerical simulation cases were conducted to study the effect of multiphase fluid flow on sand production with different sieve sizes. The water is injected with constant velocity in the oil-saturated reservoir, reproducing the secondary recovery techniques [25]. The exact initial and boundary conditions were used for all cases. The sieve size directly affects DEM particles, finally changing flow behavior during two-way coupling.

The cumulative produced sand particles and oilcut were plotted in log scale in *Figure 4*. Sand production for the *no_sieve* case increases fast and after 0.21 s becomes constant, which can define a transient sand production phenomenon [10]. This observation is consistent with sand production pattern in Ustuyrt-Buzachi oilfields (*Figure 1*). The same but deferred in time sand production trends are observed in *3dmax* and *2.5dmax* cases. The presence of a sieve only decreases the sand rate but couldn't hold particles in the reservoir. The good sand holdup effect is observed in cases *1.5dmax* and *2dmax*. The sand particles are still smaller than the sieve sizes, however due to micromechanics of particle interactions and flow distribution, the produced sand mass is still less than 1% (*Tab.4*).

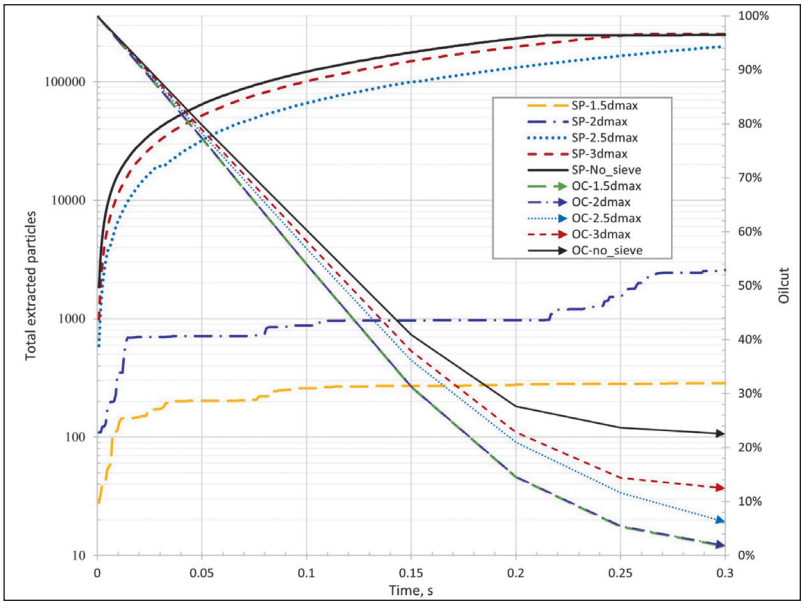

Figure 4 – **Sand production VS time**

The oilcut parameter, in this study, defined as the fraction of oil in the whole cubic spacemen (*Figure 2*) and calculated as:

$$OC = V_{oil}/V_{total} \quad (11)$$

where V_{oil} is volume of oil and V_{total} is total volume of the cubic sample. In all cases, the oilcut behavoiur shows a positive effect of sieve installation. The final oilcut for the

whole cubic sample deacreases from 23% for *no_sieve* to 2% for 1.5dmax cases, which means the oil recovery factor impoves up to 21%. The reduction of sieve size up *2dmax* sufficiently affects the final oilcut, but at the same time, further sieve size desresing doesn't improve anything. The final (at t=0.3s) sand production and oil recovery simulation results are tabulated in *Tab.4*.

Table 4 – **The final simulations result**

Case	*1,5dmax*	*2dmax*	*2,5dmax*	*3dmax*	*3,5dmax*
Sieve diameter in d50	2.322	3.096	3.870	4.643	-
Produced Sand mass, %	0.07%	0.59%	45.71%	58.39%	57.04%
Oil recovery factor	98%	98%	94%	88%	77%

It is interesting to note that, the biggest sand mass was produced in the 3dmax case and equal to 58.39%, compared to the *no_sieve* case with 57.04% of produced sand mass. This can be explained by fingering and water coning phenomena, associated with a high mobility of water to heavy oil and nonuniform displacement [26]. In the cases *2.5dmax* and *3dmax*, the sieve couldn't directly stop the sand production, but sidewards improve finale oil cut up to 88% and 94% correspondingly.

In this study, the numerical DEM sample was generated based on natural rock from the Ustuyrt-Buzachi sedimentary basin [24]. Still, due to the complexity of DEM modelling, only eight particle templates were chosen. The *d50* (mean particle size of the sample) of the numerical sample is the same to the real reservoir. The sieve size in *d50* shown in *Tab 4*. The sand particles were held on by implementing a sieve with diameters up to 3.096·d50, which is provides the highest oil recovery factor about 98%.

Conclusions. In this study, we applied coupled CFD-DEM modeling to investigate the sand production and oil recovery behavior in multiphase flow through a cubic sandstone sample. The DEM model was based on our previous studies of sand production modeling in Kazakhstan [15-16], and the properties of heavy oil from the Ustuyrt-Buzachi oilfields were selected to simulate sand particle extraction in the traditional vertical producing wells.

The transient behavior of sand production observed in simulations without a sieve qualitatively matched findings from existing literature. Sieve size played a critical role in controlling sand extraction, with smaller sieve sizes leading to lower sand production rates. Effective sand control was achieved with sieve diameters up to 3·*d50* (average particle diameter), but further increases in sieve size did not halt sand production.

The implementation of a sieve had a dual effect: it managed sand production while also enhancing the final oil recovery factor up to 21%. Even when the sieve did not fully stop sand production, it still positively influenced the oil recovery factor. A more detailed microscopic investigation of these observed phenomena will be presented in our future publication.

The developed methodology of sieve selection will be used as the sand prediction and control technique for the traditional vertical-producing wells in the Uytas oilfield, whose reservoir properties (porosity, rock permeabilities, overburden stresses, high viscous oil, etc.) are quite similar to Ustuyrt-Buzachi oilfields.

Acknowledgement. *This research was fully supported by grant AP23488951 "Enhanced oil recovery technologies improvement in reservoir with high viscosity oil" of Ministry of Science and Higher Education of the Republic of Kazakhstan. The authors gratefully acknowledge Assistant Professor Yerlan Amanbek and Research Assistant Daniyar Kazidenov from Nazarbayev University for their contributions to research and access to the software.*

REFERENCES

1 A. Acock, A. ORourk, D. Shirmboh, J. Alexander, G. Andersen, and J. López-de-Cárdenas, 'Practical Approaches to Sand Management', Oil Field Review, vol. 16, pp. 10–27, 2004, Online. Available: http://www.slb.com/~/media/Files/resources/oilfield_review/ors04/spr04/02_sand_management.pdf

2 M. B. Geilikman, M. B. Dusseault, and F. A. Dullien, 'Sand Production as a Viscoplastic Granular Flow', in Proceedings of SPE Formation Damage Control Symposium, Society of Petroleum Engineers, Feb. 1994, pp. 41–50. doi: 10.2523/27343-MS.

3 C. A. M. Veeken, D. R. Davies, C. J. Kenter, and A. P. Kooijman, 'Sand production prediction review. Developing an integrated approach', Proceedings - SPE Annual Technical Conference and Exhibition, vol. Pi, no. pt 1, pp. 335–346, 1991, doi: 10.2523/22792-ms.

4 J. Tronvoll and E. Fjær, 'Experimental study of sand production from perforation cavities', International Journal of Rock Mechanics and Mining Sciences & Geomechanics Abstracts, vol. 31, no. 5, pp. 393–410, Oct. 1994, doi: 10.1016/0148-9062(94)90144-9.

5 S. Mondal, M. M. Sharma, R. M. Hodge, R. a Chanpura, M. Parlar, and J. a Ayoub, 'A New Method for the Design and Selection of Premium / Woven Sand Screens', no. 2010, 2011.

6 M. Parlar, R. J. Tibbles, B. Gadiyar, and B. Stamm, 'A New Approach for Selecting Sand-Control Technique in Horizontal Openhole Completions', SPE Drilling & Completion, vol. 31, no. 01, pp. 004–015, Mar. 2016, doi: 10.2118/170691-PA.

7 A. Abishev, V. Tokarev, and M. Sagyndikov, 'Evaluation of In-Situ Combustion Efficiency in Karazhanbas Oilfield, Western Kazakhstan', in Day 2 Thu, November 01, 2018, SPE, Oct. 2018, pp. 1–10. doi: 10.2118/192553-MS.

8 P. M. Collins, M. B. Dusseault, D. Dorscher, and E. Kueber, 'Implementing CHOPS in the Karazhanbas Heavy Oil Field, Kazakhstan', World Heavy Oil Congress, 2008, Online. Available: http://www.petroleumgeomechanics.com/papers/Collins et al. WHOC 2008-500.pdf

9 Z. Nie, X. Zheng, and C. Xie, 'New Cementing Technologies Successfully Solved the Problems in Shallow Gas, Low Temperature and Easy Leakage Formations of North Buzachi Oilfield', in International Oil and Gas Conference and Exhibition in China, Society of Petroleum Engineers, Apr. 2010. doi: 10.2118/131810-MS.

10 F. Khamitov, 'Numerical modelling of multiphase flow in poorly consolidated sandstone reservoirs', Nazarbayev University, 2022. Online. Available: https://nur.nu.edu.kz/handle/123456789/6111

11 Y. Tsuji, T. Kawaguchi, and T. Tanaka, 'Discrete particle simulation of two-dimensional fluidized bed', Powder Technol, vol. 77, no. 1, pp. 79–87, Oct. 1993, doi: 10.1016/0032-5910(93)85010-7.

12 Z. Y. Zhou, A. B. Yu, and S. K. Choi, 'Numerical simulation of the liquid-induced erosion in a weakly bonded sand assembly', Powder Technol, vol. 211, no. 2–3, pp. 237–249, 2011, doi: 10.1016/j.powtec.2011.04.029.

13 D. Kazidenov, F. Khamitov, and Y. Amanbek, ‘Coarse-Graining Methods for the Modified JKR Contact Model on a Triaxial Compression Test’, in All Days, ARMA, Jun. 2022. doi: 10.56952/ARMA-2022-2211.

14 F. Khamitov, N. H. Minh, and Y. Zhao, ‘Numerical investigation of sand production mechanisms in weak sandstone formations with various reservoir fluids’, International Journal of Rock Mechanics and Mining Sciences, vol. 154, no. February, p. 105096, Jun. 2022, doi: 10.1016/j.ijrmms.2022.105096.

15 F. Khamitov, N. H. Minh, and Y. Zhao, ‘Coupled CFD–DEM numerical modelling of perforation damage and sand production in weak sandstone formation’, Geomechanics for Energy and the Environment, vol. 28, no. xxxx, p. 100255, Dec. 2021, doi: 10.1016/j.gete.2021.100255.

16 D. Kazidenov, F. Khamitov, and Y. Amanbek, ‘Coarse-graining of CFD-DEM for simulation of sand production in the modified cohesive contact model’, Gas Science and Engineering, vol. 113, May 2023, doi: 10.1016/j.jgsce.2023.204976.

17 Z. Y. ZHOU, S. B. KUANG, K. W. CHU, and A. B. YU, ‘Discrete particle simulation of particle–fluid flow: model formulations and their applicability’, J Fluid Mech, vol. 661, pp. 482–510, Oct. 2010, doi: 10.1017/S002211201000306X.

18 P. A. Cundall and O. D. L. Strack, ‘A discrete numerical model for granular assemblies’, Geotechnique, vol. 29, no. 1, pp. 47–65, 1979, doi: 10.1680/geot.1980.30.3.331.

19 K. L. Johnson, K. Kendall, and A. D. Roberts, ‘Surface energy and the contact of elastic solids’, Proceedings of the Royal Society of London, vol. 324, no. 1558, pp. 301–313, 1971, doi: 10.1098/rspa.1971.0141.

20 C. Goniva, C. Kloss, N. G. Deen, J. A. M. Kuipers, and S. Pirker, ‘Influence of rolling friction on single spout fluidized bed simulation’, Particuology, vol. 10, no. 5, pp. 582–591, 2012, doi: 10.1016/j.partic.2012.05.002.

21 C. W. Hirt and B. D. Nichols, ‘Volume of fluid (VOF) method for the dynamics of free boundaries’, J Comput Phys, vol. 39, no. 1, pp. 201–225, Jan. 1981, doi: 10.1016/0021-9991(81)90145-5.

22 U. Çalışkan and S. Mišković, ‘Analysis of particle dispersion and cavity formation during bulk particle water entry using fully coupled CFD-DEM-VOF approach’, Particuology, vol. 90, pp. 558–580, 2024, doi: 10.1016/j.partic.2023.12.018.

23 R. Di Felice, ‘The voidage function for fluid-particle interaction systems’, International Journal of Multiphase Flow, vol. 20, no. 1, pp. 153–159, 1994, doi: 10.1016/0301-9322(94)90011-6.

24 A. D. Shabdirova, Z. Bissekenova, N. H. Minh, and J. R. Kim, ‘Sample preparation method of clay-rich sandstone analogue of sandstone reservoirs in Kazakhstan’, in 50th US Rock Mechanics / Geomechanics Symposium 2016, 2016.

25 J. R. Fanchi, ‘Improved Recovery’, in Shared Earth Modeling, Elsevier, 2002, pp. 272–281. doi: 10.1016/B978-075067522-2/50016-1.

26 Z. Kargozarfard, M. Riazi, and S. Ayatollahi, ‘Viscous fingering and its effect on areal sweep efficiency during waterflooding: an experimental study’, Pet Sci, vol. 16, no. 1, pp. 105–116, Feb. 2019, doi: 10.1007/s12182-018-0258-6.